Available online at www.sciencedirect.com
ScienceDirect
Thin Solid Films 516 (2008) 1082–1087
www.elsevier.com/locate/tsf

Nano-indentation of hybrid silica coatings on surgical grade stainless steel

Josefina Ballarre [a,b,*], Damián A. López [a], Ana L. Cavalieri [b]

[a] Corrosion Division-Material's Science and Technology Research Institute (INTEMA), UNMdP-CONICET, Juan B. Justo 4302, B7608FDQ, Mar del Plata, Argentina
[b] Ceramics Division/Structural Materials Laboratory-Material's Science and Technology Research Institute (INTEMA), UNMdP-CONICET, Juan B. Justo 4302, B7608FDQ, Mar del Plata, Argentina

Received 14 December 2006; received in revised form 19 June 2007; accepted 29 July 2007
Available online 7 August 2007

Abstract

Hybrid silica-based coatings with tetraethoxysilane (TEOS), methyltrietoxysilane (MTES), hydroxyethyl-methacrylate (HEMA) and methacrylopropyl-trimethoxysilane (γMPS) as precursors, were employed to improve the performance of stainless steel used as orthopaedic material. Mechanical properties of the films, such as Young's modulus and hardness, were studied using the load and depth sensing indentation technique known as nano-indentation. The elastic/plastic and creep behaviours were also analyzed. Coatings with a high proportion of organic components (HEMA, γMPS) presented a more plastic response compared to the more vitreous coatings (containing only TEOS and MTES). They also showed the lowest Young's modulus and hardness. Therefore, the more vitreous coatings presented lower creep deformation that increased with the load applied.

Keywords: Hybrid coating; Sol–gel; Mechanical properties; Silicon oxide; Nano-indentation

1. Introduction

Metals are widely used in orthopaedic surgery due to their important mechanical properties [1]. However, they are not able to create a natural union with the mineralized bone and may release metallic particles causing different pathologies that could ultimately require the removal of the implant [2,3]. One way to improve the performance of metallic implants is to apply a protective film [4,5]. These coatings are mainly made from alcoxide precursors of SiO_2 that create vitreous films. These films can be bioactive or be functionalized with the addition of bone-growth-inducing particles [6–10].

A disadvantage of glassy coatings is their brittleness. Hybrid organic–inorganic films with a high content of silica are presented as an alternative to improve the mechanical response of the vitreous coatings while preserving one of their interesting qualities: to be a protective and dense network [11,12]. The incorporation of hydroxides with some organic groups is expected to give plastic characteristics to the films. Organic compounds such as methacrylopropyl-trimethoxysilane (γMPS) or hydroxyethyl-methacrylate (HEMA) have been recently used to obtain thicker hybrid coatings [13].

Although mechanical properties of hybrid organic–inorganic sol–gel films have been studied [14–16], there is not much

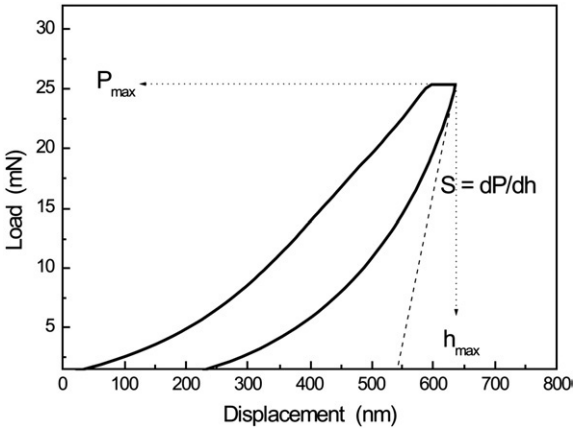

Fig. 1. Typical load–unloading vs. displacement curve showing the maximum tip penetration (h_{max}), the maximum applied load (P_{max}), the final depth (h_f) and the system stiffness (S).

* Corresponding author. Juan B. Justo 4302, B7608FDQ, Mar del Plata, Argentina. Tel.: +54 223 481 6600; fax: +54 223 4810046.
E-mail address: jballarre@fi.mdp.edu.ar (J. Ballarre).

0040-6090/$ - see front matter © 2007 Elsevier B.V. All rights reserved.
doi:10.1016/j.tsf.2007.07.186

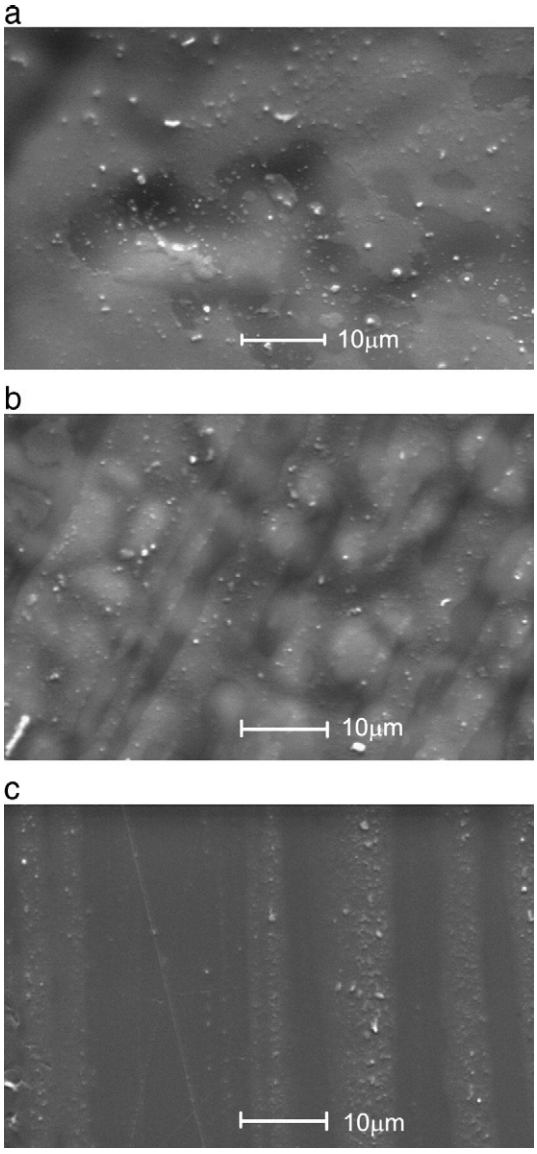

Fig. 2. SEM images of (a) TEOS–MTES, (b) THM coatings, and (c) TEOS–MTES/TMH dual coating on SS316L substrate.

information about their Young's modulus or hardness. These are key parameters in the study of the adhesion of thin films to metallic substrates and their response to mechanical loads.

One of the technique most recently used to study the mechanical properties of thin films is the instrumented indentation, known as nano-indentation. This is a superficial technique to quasi-statically measure the penetration generated by increasing loads applied to a material.

The objective of this work is to employ nano-indentation to characterize the mechanical properties of hybrid organic–inorganic silica-based thin coatings deposited on stainless steel used in orthopaedic surgery.

2. Experimental procedure

Flat samples (30×30 mm^2) of stainless steel AISI 316L were used as substrates. The substrates were cleaned in soap solution, in isopropylic alcohol and in an ultrasound bath for 5 min after rising with destilated water. Then they were dried with hot air before the application of the coating.

Two types of sols were used for the coatings: TEOS (Tetraethoxysilane)-MTES (Methyltrietoxysilane) and TMH (TEOS (Tetraethoxysilane)-γMPS (3-methacrylopropyl-trimethoxysilane)-HEMA (2-hydroxyethyl-methacrylate)). The TEOS–MTES sol was prepared by acid catalysis method in one stage, using TEOS (ABCR), and MTES (ABCR) as silica precursors; absolute ethanol as solvent and nitric and acetic acids (0.1 N) as catalysts. The water, needed for the hydrolysis, was incorporated from the nitric acid solution in stoichiometric ratio. The molar ratio of TEOS/MTES was 40:60. All the reagents were stirred at 40 °C during 3 h obtaining a transparent sol (pH = 1–2, viscosity = 2.6 mPa s). The TEOS (ABCR)-γMPS (Dow Corning)-HEMA (Aldrich)) (TMH) sol was made in a two steps procedure using 0.1 N nitric acid and isopropylic alcohol. The solution, containing 40 g l^{-1} of SiO_2, was stirred at 65 °C for 36 h in a glycerine bath.

Coatings were obtained by dip-coating at room temperature using a withdraw rate of 25 cm min^{-1}. Three different types of coatings were applied on the substrates:

(a) Single coating consisting on one layer of TEOS–MTES sol treated at 450 °C for 30 min in air.

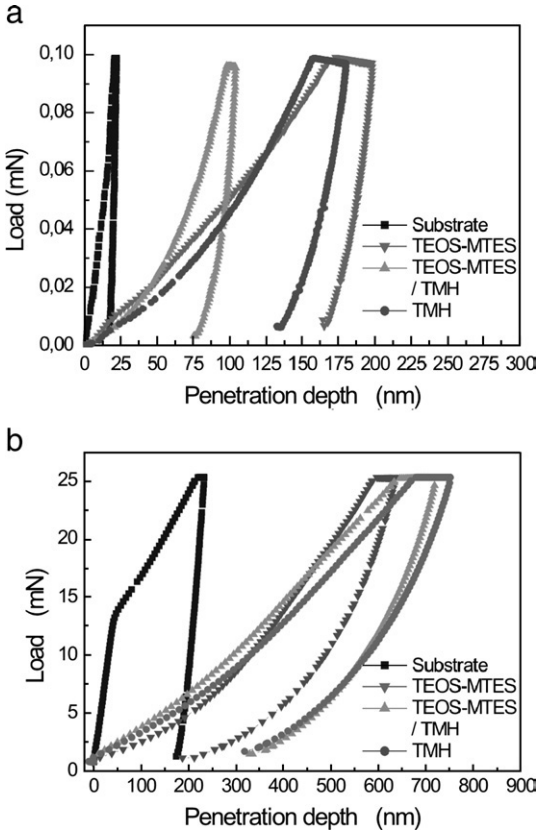

Fig. 3. Load–unload vs. displacement curves for the three coatings and the substrate tested with a maximum load of 0.1 (a) and 25 mN (b). The typical SS316L behaviour is also shown.

(b) Single coating consisting on two layers of TMH sol applied successively. The first layer was dried 30 min in air and the second was treated at 150 °C for 60 min in air.
(c) Double coating consisting on a first layer of the TEOS–MTES hybrid treated at 450 °C during 30 min in air (type a), followed by a second double layer of TMH (type b) coating, treated at 150 °C 60 min in air.

The surfaces of the coatings were examined by scanning electron microscopy (SEM) using a Phillips XL30 equipment with an operating voltage of 20 kV.

The mechanical properties of the silica-based films were studied using the nano-indentation technique. Both the Young's modulus and the hardness were determined and other relevant data of the films were analyzed from the load-displacement curves [17]. A Nanoindenter XP (MTS Nano Instruments) with a three-side pyramid Berkovich indenter was used. Multiple indentations (a matrix of 4 × 4) separated by 100 μm were made in each sample. Increasing maximum loads were used in each indentation (total of 9), obtaining multiple curves for different penetrations. A complete cycle of loading–unloading with maximum loads from 0.1 to 50 mN and a load hold time of 15 s were employed. The calibration of the indenter shape was performed using fused silica.

The analysis of indentation load-penetration curves produced by instrumented indentation systems is often based on work by Oliver and Pharr [17], and based upon relationships developed by Sneddon [18].The results were analyzed according to the equation:

$$S = 2aE_r = \frac{2\beta}{\sqrt{\pi}} E_r \sqrt{A}, \tag{1}$$

where a is the contact radius and A is the protected area of the tip sample contact. β is used to account for the triangular and square cross sections of many indenters used in nano-indentation studies. The values of β for different indenters were determined by King [19] and other authors. For a Berkovich indenter, $\beta = 1.096$ [20,21].

The stiffness (S) was determined as the slope $S = dP/dh$ of the upper portion of the unloading curve, where P is the applied load and h is the displacement. Fig. 1 shows a schematic graph of load vs. indenter displacement data for an indentation test where h_{max} is the maximum displacement at maximum applied load P_{max} and h_f is the final depth of the contact impression after unloading. E_r is the reduced modulus defined through the equation:

$$\frac{1}{E_r} = \frac{(1-\nu^2)}{E} + \frac{(1-\nu_i^2)}{E_i}, \tag{2}$$

where E and ν are the Young's modulus and Poisson's ratio of the specimen, and E_i and ν_i are the modulus and ratio for the

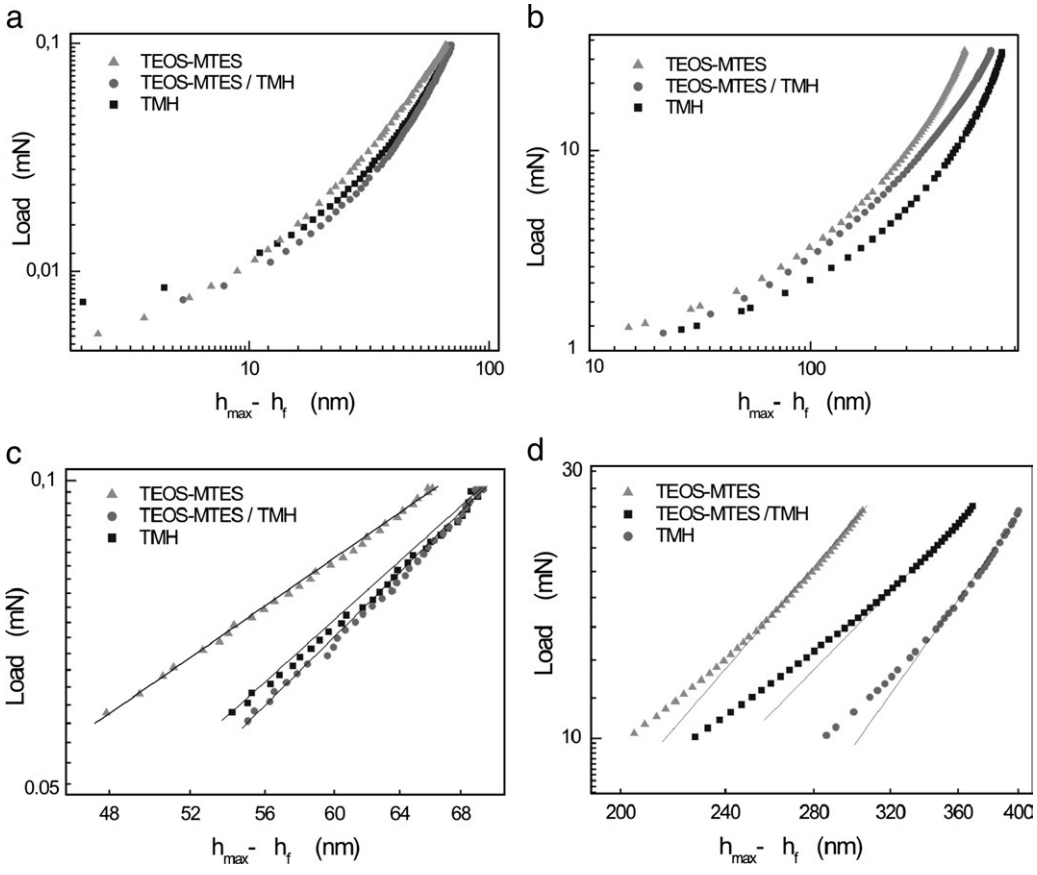

Fig. 4. Unload vs. penetration depth logarithmic graphs of the three types of coatings at P_{max} equal to 0.1 mN (a) and 25 mN (b), and upper portion of the same curves at P_{max} equal to 0.1 mN (c) and 25 mN (d).

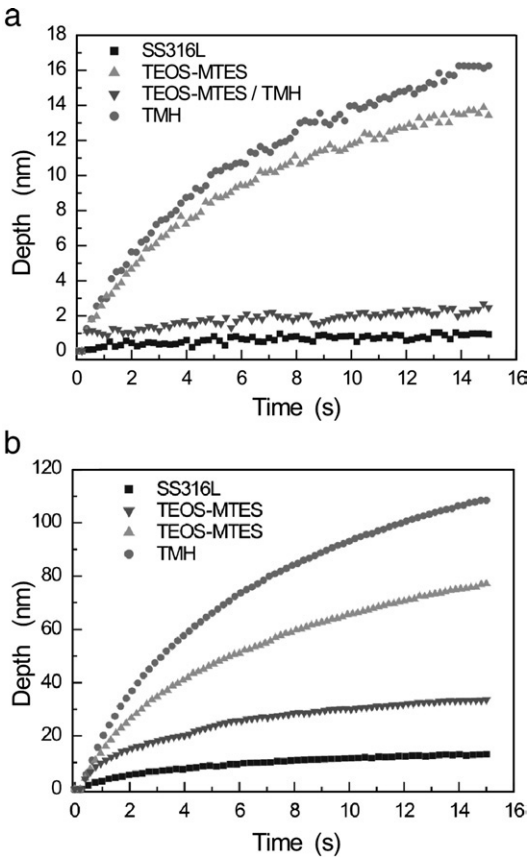

Fig. 5. Creep behaviour of TEOS–MTES, TEOS–MTES/TMH, TMH coatings and SS316L with an applied loads of 0.1 mN (a) and 25 mN (b).

indenter (E_i=1140 GPa and ν_I=0.07 for a diamond Berkovich type indenter). For all samples a Poisson's ratio equal to 0.25 was used.

The hardness was determined using the equation:

$$H = \frac{P_{max}}{A_c}, \tag{3}$$

where A_c is the area of the indentation at a maximum applied load, P_{max}. By knowing precisely the geometry of the indenter (by calibration), A_c can be expressed in terms of the contact depth h_c directly determined from measurements.

3. Results and discussion

The images of the three types of coatings obtained by scanning electronic microscopy (SEM) are presented in Fig. 2. The surfaces are homogeneous with no presence of flaws. Good adaptability of the coating to the substrates and their imperfections was observed (and this fact could probably achieve good integrity of them).

For the load-displacement measurements of the nano-indentation tests, typical load–unloading curves were obtained. The results for the three types of coatings as well as for the substrate for two of the maximum loads employed (0.1 and 25 mN, respectively) are presented in Fig. 3. When the lower P_{max} (0.1 mN) was applied, the highest final penetration h_f (93 nm) was obtained for the TMH coating in which the organic concentration was high. The lowest final penetration corresponded to the TEOS–MTES coating (21 nm), similar to the value of the substrate (13 nm). The TEOS–MTES/TMH presented an intermediate value (81 nm). These h_f values indicate a decrease in the plastic character of the coatings in the order TMH > TEOS–MTES/TMH > TEOS–MTES. At high P_{max} (25 mN) permanent deformation was observed for the three type of coatings. Typical curves for the metallic substrate (stainless steel) were registered as comparative data. The use of sharp indenters, as Berkovich, induces very high stress for low loads as compared to other type of indenters [22]. The plastic zone, especially in metals, is very small and is difficult to recognize with optical or SEM images. In this case we assumed that the offset of plasticity is only reached at high loads because of the non-superposition of the loading and unloading curve.

In order to analyze the elastic/plastic behaviour of the coatings, we used a model employing the modified power law equation [23]:

$$P = \alpha(h - h_f)^m, \tag{5}$$

where P is the applied load, $(h-h_f)$ is the total elastic recovery during unloading, and α and m are constants that depend on the material. In Fig. 4a and b, the unloading curves for all the coatings at P_{max} of 0.1 and 25 mN are plotted as a function of the final elastic displacement $(h_{max}-h_f)$. For the three types of coatings studied, a clear non-linearity in the entire range of applied loads is observed. The power law can only be applied in the upper portion of the curves (Fig. 4c and d, respectively). At the highest maximum load (25 mN), the power law (for an elastic behaviour) is only valid in a narrow range. For P_{max}=0.1 mN, values of m between 1.5 and 2.2 and for α, values between 1.5×10^{-4} to 8.8×10^{-6} were found, the lowest values corresponding to the TOES–MTES coatings. The highest values of m could be related to non-elastic effects [24,25]. This suggests that, during the beginning of under-loading at high loads, another event contributes to the deformation process. To obtain more information from indentation curves it is necessary to treat the Berkovich indentation as a full three-dimensional problem [26].

From the analysis of the above results, a dominant elastic behaviour of the studied materials can be considered when low

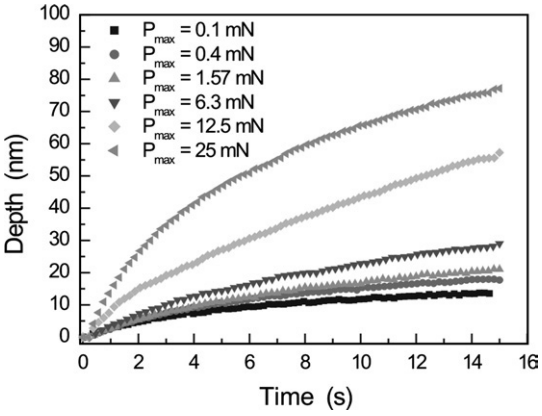

Fig. 6. Creep behaviour of TEOS–MTES/TMH coating at several P_{max} applied.

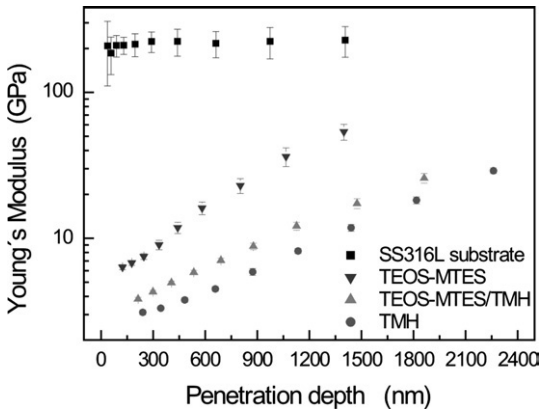

Fig. 7. Young's modulus profiles of TEOS–MTES, TEOS–MTES/TMH, TMH coatings and the substrate SS AISI 316L.

maximum loads are applied. Conversely, plastic deformation is the main contribution observed from the beginning of the unload curve at the higher load (25 mN). The penetration displacements prior to unloading, when the maximum load is maintained during a given time, are due to creep (Fig. 3).This sample deformation as a function of time has been analyzed for materials subjected to the same load conditions during 15 s. The behaviour of the three types of coatings at two loads (0.1 or 25 mN) are compared with that of the substrate (Fig. 5a and b, respectively). For all coatings, the deformation is highly dependent on the applied load. At the lower load, the deformation by creep of the TMH coating in addition to its plastic response is larger than that of TEOS–MTES/TMH one. The silica-based film (TEOS–MTES) showed a similar behaviour to SS316L: small time dependent deformation and prevalence of elastic response after the initial loading. At the higher load, the plastic deformation induced by creep was larger for the TEOS–MTES than the one at the lower load. In Fig. 6 the creep behaviour of the dual coating TEOS–MTES/TMH at different maximum loads in the entire range studied is also showed. As expected, an increment in creep deformation at higher applied P_{max} was observed for the studied load range. The maximum deformation reached, for P_{max} of 6.3 mN (or lower), was less than 30 nm;

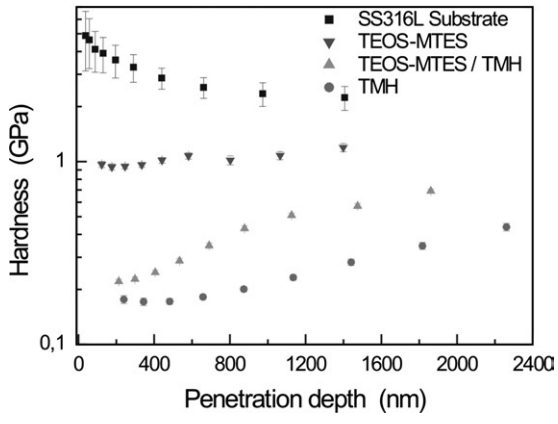

Fig. 8. Hardness profiles of TEOS–MTES, TEOS–MTES/TMH, TMH coatings and the substrate SS AISI 316L.

Table 1
Young's modulus and hardness of the three types of studied coatings, the substrate and other referenced materials

Material	Young's modulus (GPa)	Hardness (GPa)
SS316L	212	2.3
TEOS–MTES	6.5	0.92
TEOS–MTES/TMH	3.8	0.22
TMH	3	0.16
Soda-lime glass	70 [a]	6 [a]
Aluminium	78 [a]	0.3 [a]

[a] From Oliver and Pharr [17].

however, when the load was doubled (12.5 mN), the deformation was affected by a factor of 2.

From comparison of the indentation data of the three types of coatings and the data from the substrate, both the Young's modulus (E) and the hardness (H) as a function of depth penetration can be obtained with the equations from the Oliver and Pharr model and their corrections for the upper fraction of the curve (Figs. 7 and 8, respectively). The assumption that the values are not influenced by the substrate was made [27]. A large number of models and methods could be used to deduce some mechanical properties of the coated materials. In this work, Young's modulus and hardness of the coatings were estimated from depth profile data at 10% of the film thickness (Table 1). It is noteworthy that this 10% rule of thumb does not take into account the particular properties of the hard substrate and the soft film used, nor the deformation mechanisms involved during the indentation. Other values of E and H of typical plastic (aluminium) and elastic (soda-lime glass) materials measured by indentation [17] were also included in the table, for comparison.

The unflawed state is quite important for biomedical applications in order to avoid corrosion or wear events. In all of the samples analyzed no film cracking was observed after indentation. However it has to be considered that low loads were applied.

A remarkable rise in the Young's modulus values with the increase of penetration depth is observed in Fig. 7. A similar dependence can be observed with the hardness for the TMH and TEOS–MTES/TMH coatings in Fig. 8. This behaviour could be attributed to the influence of the elastic characteristics of the substrate. The coating with the highest amount of organic components (TMH) showed the lower superficial modulus and hardness. This fact was attributed to the increase of polymeric network formed induced by the 2-hydroxyethyl-methacrylate (HEMA). The most vitreous coating (TEOS–MTES) showed the highest elastic modulus and hardness. These values can be associated to the different degree of elasticity of the coatings as presented above.

4. Conclusions

The three kinds of coatings show different degrees of elastic recovery during unloading, the largest being that for TEOS–MTES. Most of the indenter displacement in the other two coatings, TEOS–MTES/TMH and TMH, is rearranged plastically and only a small portion is recovered on unloading.

In the course of the holding process, the amount of creep deformation reached is less significant with low loads. The values of Young's modulus, hardness, and the penetration depth, increase when the content of the organic components in the coating increases. The creep deformation is higher with an increase of the amount of organic components, as well.

Acknowledgments

The authors would like to thank Dr. Paulo Cesar Soares Jr. from the Nanomechanical Properties Laboratory-UFPR, Brazil for the experimental help and the SECyT-CAPES cooperation research program and the ANPCyT-Argentina PICTO 11338 project, for the financial support.

References

[1] J.B. Park, Biomaterials Science and Engineering, Plenum Press, New York, 1984.
[2] Y. Okazaki, E. Gotoh, T. Manabe, K. Kobayashi, Biomaterials 25 (2004) 5913.
[3] J. Woodman, J. Black, D. Nunamaker, J. Biomed. Mater. Res. 17 (1983) 655.
[4] J. de Damborenea, N. Pellegri, O. de Sanctis, A. Durán, J. Sol–Gel Sci. Technol. 4 (1995) 239.
[5] P.G. Galliano, J. de Damborenea, M.J. Pascual, A. Durán, J. Sol–Gel Sci. Technol. 13 (1998) 723.
[6] P. Li, K. de Groot, T. Kokubo, J. Sol–Gel Sci. Technol. 7 (1996) 27.
[7] C. Ohtsuki, T. Kokubo, T. Yamamuro, J. Non-Cryst. Solids 143 (1992) 84.
[8] O. Peitl, E.D. Zanotto, L.L. Hench, J. Non-Cryst. Solids 292 (2001) 115.
[9] X. Liu, C. Ding, P. Chu, Biomaterials 25 (2004) 1755.
[10] T. Kokubo, H. Kim, M. Kawashita, Biomaterials 24 (2003) 2161.
[11] L.E. Amato, D.A. López, P.G. Galliano, S.M. Ceré, Mater. Lett. 59 (2005) 2026.
[12] J. Ballarre, J.C. Orellano, C. Bordenave, P.G. Galliano, S.M. Ceré, J. Non-Cryst. Solids 304 (2002) 278.
[13] S.A. Pellice, U. Gilabert, C. Solier, Y. Castro, A. Durán, J. Non-Cryst. Solids 348 (2004) 172.
[14] R. Prikryl, V. Cech, L. Zajickova, J. Vanek, S. Behzadi, F.R. Jones, Surf. Coat. Technol. 200 (2005) 468.
[15] J. Malzbender, G. de With, J.M.J. den Toonder, Thin Solid Films 366 (2000) 139.
[16] V. Soloukhin, W. Posthumus, J. Brokken-Zijp, J. Loos, G. de With, Polymer 43 (2002) 6169.
[17] W.C. Oliver, G.M. Pharr, J. Mater. Res. 7 (1992) 1564.
[18] I.N. Sneddon, Int. J. Eng. Sci. 3 (1965) 47.
[19] R.B. King, Int. J. Solids Struct. 23 (1987) 1657.
[20] M. Dan, N. Chollacoop, K.J. Van Vliet, T.A. Venkatesh, S. Suresh, Acta Mater. 49 (2001) 3899.
[21] A.C. Fischer-Crippers, Surf. Coat. Technol. 200 (2006) 153.
[22] B. Wolf, Cryst. Res. Technol. 35 (2000) 377.
[23] M.F. Doerner, D.S. Gardner, W.D. Nix, J. Mater. Res. 1 (1986) 845.
[24] F. Mammeri, E. Le Bourhis, L. Rozes, C. Sanchez, A. Hugnard, D. Lefevre, J. Non-Cryst. Solids 345 (2004) 610.
[25] F. Mammeri, E. Le Bourhis, L. Rozes, C. Sanchez, J. Eur. Ceram. Soc. 26 (2006) 259.
[26] J. Woirgard, J.-C. Dargenton, C. Tromas, V. Audurier, Surf. Coat. Technol. 100–101 (1998) 103.
[27] B.N. Lucas, C.T. Rosenmayer, W.C. Oliver, Mater. Res. Soc. Symp. Proc. 505 (1998) 97.